

High quality factor silica microspheres functionalized with self-assembled nanomaterials

Ishac Kandas,^{1,2,*} Baigang Zhang,¹ Chalongrat Daengngam,³ Islam Ashry,^{1,2} Chih-Yu Jao,³ Bo Peng,⁴ Sahin K. Ozdemir,⁴ Hans D. Robinson,³ James R. Heflin,³ Lan Yang,⁴ and Yong Xu^{1,5}

¹ The Bradley Department of Electrical and Computer Engineering, Virginia Tech, Blacksburg, Virginia 24061, USA.

² Department of Engineering Mathematics and Physics, Faculty of Engineering, Alexandria University, Alexandria 21526, Egypt

³ Department of Physics, Virginia Tech, Blacksburg, Virginia 24061, USA.

⁴ Department of Electrical and Systems Engineering, Washington University in St. Louis, Missouri 63130, USA.

⁵yong@vt.edu

*ishac@vt.edu

Abstract: With extremely low material absorption and exceptional surface smoothness, silica-based optical resonators can achieve extremely high cavity quality (Q) factors. However, the intrinsic material limitations of silica (e.g., lack of second order nonlinearity) may limit the potential applications of silica-based high Q resonators. Here we report some results in utilizing layer-by-layer self-assembly to functionalize silica microspheres with nonlinear and plasmonic nanomaterials while maintaining Q factors as high as 10^7 . We compare experimentally measured Q factors with theoretical estimates, and find good agreement.

©2013 Optical Society of America

OCIS codes: (060.3510) Lasers, fiber; (140.4780) Optical resonators.

References and links

1. M. L. Gorodetsky, A. A. Savchenkov, and V. S. Ilchenko, "Ultimate Q of optical microsphere resonators," *Opt. Lett.* **21**(7), 453–455 (1996).
2. A. B. Matsko and V. S. Ilchenko, "Optical resonators with whispering-gallery modes-part I: basics," *IEEE J. Quantum Electron.* **12**(1), 3–14 (2006).
3. K. J. Vahala, "Optical microcavities," *Nature* **424**(6950), 839–846 (2003).
4. J. Zhu, S. K. Ozdemir, Y.-F. Xiao, L. Li, L. He, D.-R. Chen, and L. Yang, "On-chip single nanoparticle detection and sizing by mode splitting in an ultrahigh- Q microresonator," *Nat. Photonics* **4**(1), 46–49 (2010).
5. H. C. Ren, F. Vollmer, S. Arnold, and A. Libchaber, "High- Q microsphere biosensor - analysis for adsorption of rodlike bacteria," *Opt. Express* **15**(25), 17410–17423 (2007).
6. G. Kozyreff, J. L. Dominguez-Juarez, and J. Martorell, "Nonlinear optics in spheres: from second harmonic scattering to quasi-phase matched generation in whispering gallery modes," *Laser Photon. Rev.* **5**(6), 737–749 (2011).
7. T. J. Kippenberg and K. J. Vahala, "Cavity opto-mechanics," *Opt. Express* **15**(25), 17172–17205 (2007).
8. J. D. Suter, Y. Sun, D. J. Howard, J. A. Viator, and X. Fan, "PDMS embedded opto-fluidic microring resonator lasers," *Opt. Express* **16**(14), 10248–10253 (2008).
9. Y. Xu, A. Wang, J. R. Heflin, and Z. Liu, "Proposal and analysis of a silica fiber with large and thermodynamically stable second order nonlinearity," *Appl. Phys. Lett.* **90**(21), 211110 (2007).
10. S. I. Shopova, C. W. Blackledge, and A. T. Rosenberger, "Enhanced evanescent coupling to whispering-gallery modes due to gold nanorods grown on the microresonator surface," *Appl. Phys. B* **93**(1), 183–187 (2008).
11. Y. Xu, M. Han, A. Wang, Z. Liu, and J. R. Heflin, "Second order parametric processes in nonlinear silica microspheres," *Phys. Rev. Lett.* **100**(16), 163905 (2008).
12. T. J. Kippenberg, S. M. Spillane, B. Min, and K. J. Vahala, "Theoretical and experimental study of stimulated and cascaded Raman scattering in ultrahigh- Q optical microcavities," *IEEE J. Quantum Electron.* **10**(5), 1219–1228 (2004).
13. K. A. Willlets and R. P. Van Duyne, "Localized surface plasmon resonance spectroscopy and sensing," *Annu. Rev. Phys. Chem.* **58**(1), 267–297 (2007).

14. H. S. Choi, X. Zhang, and A. M. Armani, "Hybrid silica-polymer ultra-high- Q microresonators," *Opt. Lett.* **35**(4), 459–461 (2010).
15. M. A. Santiago-Cordoba, S. V. Boriskina, F. Vollmer, and M. C. Demirel, "Nanoparticle-based protein detection by optical shift of a resonant microcavity," *Appl. Phys. Lett.* **99**(7), 073701 (2011).
16. J. L. D. -Juarez, G. Kozyreff, and J. Martorell, "Whispering gallery microresonators for second harmonic light generation from a low number of small molecules," *Nature Commun.* **2**, 1–8 (2011).
17. A. Chiasera, Y. Dumeige, P. Feron, M. Ferrari, Y. Jestin, G. N. Conti, S. Pelli, S. Soria, and G. C. Righini, "Spherical whispering-gallery-mode microresonators," *Laser Photonics Rev.* **4**(3), 457–482 (2010).
18. A. Garg, R. M. Davis, C. Durak, J. R. Heflin, and H. W. Gibson, "Polar orientation of a pendant anionic chromophore in thick layer-by-layer self-assembled polymeric films," *J. Appl. Phys.* **104**(5), 053116 (2008).
19. K. E. Van Cott, M. Guzy, P. Neyman, C. Brands, J. R. Heflin, H. W. Gibson, and R. M. Davis, "Layer-by-layer deposition and ordering of low molecular weight dye molecules for second order nonlinear optics," *Angew. Chem. Int. Ed.* **41**(17), 3236–3238 (2002).
20. J. R. Heflin, M. T. Guzy, P. J. Neyman, K. J. Gaskins, C. Brands, Z. Wang, H. W. Gibson, R. M. Davis, and K. E. Van Cott, "Efficient, thermally stable, second order nonlinear optical response in organic hybrid covalent/ionic self-assembled films," *Langmuir* **22**(13), 5723–5727 (2006).
21. J. Yi, C.-Y. Jao, I. L. N. Kandas, B. Liu, Y. Xu, and H. D. Robinson, "Irreversible adsorption of gold nanospheres on fiber optical tapers and microspheres," *Appl. Phys. Lett.* **100**(15), 153107 (2012).
22. D. W. Vernooy, V. S. Ilchenko, H. Mabuchi, E. W. Streed, and H. J. Kimble, "High- Q measurements of fused-silica microspheres in the near infrared," *Opt. Lett.* **23**(4), 247–249 (1998).
23. F. P. Payne and J. P. R. Lacey, "A theoretical analysis of scattering loss from planar optical waveguides," *Opt. Quantum Electron.* **26**(10), 977–986 (1994).
24. C. Daengngam, M. Hofmann, Z. Liu, A. Wang, J. R. Heflin, and Y. Xu, "Demonstration of a cylindrically symmetric second-order nonlinear fiber with self-assembled organic surface layers," *Opt. Express* **19**(11), 10326–10335 (2011).
25. S. Arnold, S. I. Shopova, and S. Holler, "Whispering gallery mode bio-sensor for label-free detection of single molecules: thermo-optic vs. reactive mechanism," *Opt. Express* **18**(1), 281–287 (2010).
26. J. D. Jackson, *Classical electrodynamics*, John Wiley & Sons, Inc., 1998.
27. S. Arnold, M. Khoshima, I. Teraoka, S. Holler, and F. Vollmer, "Shift of whispering-gallery modes in microspheres by protein adsorption," *Opt. Lett.* **28**(4), 272–274 (2003).
28. C. F. Bohren and D. R. Huffman, *Absorption and Scattering of Light by Small Particles* (John Wiley & Sons, Inc., 1998).
29. I. Teraoka and S. Arnold, "Theory of resonance shifts in TE and TM whispering gallery modes by nonradial perturbations for sensing applications," *J. Opt. Soc. Am. B* **23**(7), 1381–1389 (2006).
30. P. B. Johnson and R. W. Christy, "Optical constants of the noble metals," *Phys. Rev. Lett.* **6**, 4370–4379 (1972).
31. L. He, S. K. Ozdemir, J. Zhu, F. Monifi, H. Yilmaz, and L. Yang, "Statistics of multiple-scatterer-induced frequency splitting in whispering gallery microresonators and microlasers," *New J. Phys.* **15**(7), 073030 (2013).

1. Introduction

Recently, silica-based optical whispering gallery modes (WGMs) micro-resonators have drawn much attention [1–4]. In such resonators, optical confinement is provided by total internal reflection at the circular boundary of the resonators. Due to the exceptionally low optical absorption coefficient in silica and the extremely smooth surface morphology of the resonators, the Q factors of the WGMs can often be as high as 10^{10} [1]. The high quality factor has led to many interesting applications in areas such as chemical and biological sensing [5], nonlinear optics [6], optomechanics [7], and optofluidics [8]. Despite these advantages, silica-based high Q resonators also face some intrinsic limits. For example, silica possesses neither second order nonlinearity [9] nor plasmonic resonances [10]. Consequently, it is difficult to investigate important processes such as second order parametric oscillation [11] or surface enhanced Raman scattering in such resonators [12,13]. The key to overcome this deficiency is to develop a versatile method that can functionalize the surface of a silica microsphere with various nanomaterials while maintaining high cavity Q factors. The goal of this paper is to characterize an electrostatic self-assembly based approach that can incorporate different types of functional materials onto the surface of a silica resonator with nanoscale control of thickness while maintaining high Q factors.

To the best of our knowledge, there are relatively few systematic studies on how to functionalize silica-based high- Q resonators. Relevant examples include recent demonstrations of silica high Q resonators coated with polymer [14], gold nanoparticles (Au

NPs) [10,15], and nonlinear molecules [6,16]. The method of self-assembly has several important advantages. First, by depositing one monolayer of nanomaterial at a time, the self-assembly approach can control the functionalization of silica microspheres with nanoscale accuracy and maintain exceptional surface smoothness. Second, the self-assembly approach relies on electrostatic interaction and is therefore compatible with a wide range of nanomaterials including nonlinear molecules, dyes, quantum dots, and plasmonic NPs. By selecting appropriate aqueous solutions for self-assembly, we can therefore incorporate a large variety of functional materials onto the same microsphere, which can be difficult to accomplish with alternative approaches. Finally, the self-assembly process is simple, straightforward, and can be carried out without using any specialized equipment or clean room facilities.

In this paper, we consider two types of functional materials. The first is polar ionic self-assembled multilayer (ISAM) films that possess second order nonlinearities, and the second is Au NPs that support plasmonic resonances. We fabricated multiple functional microspheres with different ISAM film thickness and Au NPs density. We find that the Q factors of these microspheres are mainly limited by optical absorption in the case of the ISAM film, and optical absorption /scattering in the case of the Au NPs. By controlling the number of polymer layers or the NP density, we can adjust the Q factors of these functional microspheres in the range of 10^6 to 10^7 . The results in this paper may also be generalized to other functional materials including various macromolecules, dyes, and non-spherical plasmonic NPs.

2. Sample fabrication and experimental setup

We fabricated silica microspheres using the procedure described in [17]. Briefly, we placed a silica fiber between two fiber clamps attached to a computer-controlled motion stage. We then used a focused high-power CO₂ laser beam to melt the silica fiber. After stretching and melting the fiber, a microsphere naturally formed from the molten silica due to surface tension. The fabrication parameters were adjusted to obtain microsphere diameters in the range of 240-260 μm .

After microsphere fabrication, we coated the silica surface with two different ISAM films that possess second order nonlinear susceptibilities. The first was composed of alternating layers of (poly (allylamine hydrochloride)) (PAH) and (poly {1-[p-(3'-carboxy-4'-hydroxyphenylazo) benzenesulfonamido]-1, 2-ethandiyl} (PCBS) and the second composed of PAH and Procion Brown (PB). ISAM films of PAH/PCBS and PAH/PB have been shown to possess net polar order and as a result, can produce substantial second order nonlinear susceptibilities [18,19]. To incorporate multiple layers of nonlinear polymers onto the silica microsphere, we can use the self-assembly procedure as follows. First, we placed the microsphere in the positively charged polycation (PAH) solution for 3 minutes followed by 2 minutes of rinsing in deionized (DI) water (the rinsing process remove excess polymer and therefore ensure uniform PAH coverage). Afterwards, we placed the microsphere in the negatively-charged polyanion solution containing PCBS (or PB) for 3 minutes to cover the PAH layer with a monolayer of PCBS (or PB). This step is again followed by 2 minutes DI water rinsing to remove any residual polyanion. Because the self-assembly relies on electrostatic interaction, the process is self-limiting, and each polymer layer with a well-defined thickness (typically 0.3 - 10.0 nm dependent on solution pH and ionic strength) is added at each deposition step. As a result, the resulting bilayer is very uniform, and can have a thickness of 1 nm or less. This process can be repeated as many times as desired to reach the desired ISAM film thickness. For this experimental study, PAH, PCBS and PB were purchased from Sigma-Aldrich. The concentrations and the pH values are respectively 0.93 mg/mL and pH \sim 7 for PAH solution, 3.7 mg/mL and pH \sim 7 for PCBS solution, and 1 mg/mL and pH \sim 10.5 for PB solution. For the fabrication of PAH/PB ISAM films, we added sodium chloride into the PB solution at a concentration of 30 mg/mL. The Na⁺ ions screen the

repulsions of the negatively-charged polyanion, thus enabling close packing of PB on the surface [20].

The assembly of Au NPs was carried out using the same principle. We first coated the silica microsphere with a monolayer of positively-charged PAH. Then we placed the PAH-coated microsphere in an aqueous solution containing negatively-charged Au NPs (30 nm in diameter, British Biocell International). The density of Au NPs adsorbed on the microsphere surface can be readily adjusted by controlling deposition time. (In [21], more details can be found, which also provided an analytical model that describes the density of adsorbed Au NPs as a function of deposition time). Figure 1 shows scanning electron microscope (SEM) images of two functional microspheres, one coated with 20 bilayers of PAH/PB, and the other covered with Au NPs. As we can see from the SEM images, the fabrication procedure described above can produce functional microspheres with very smooth surface morphology.

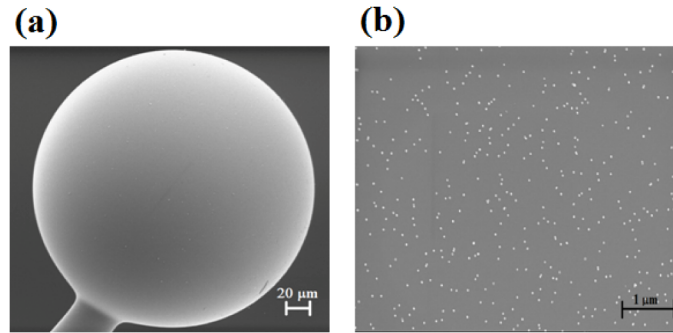


Fig. 1. SEM images of a microsphere coated with (a) 20 bilayers of PAH/PB. (b) Au NPs deposited for 20 minutes.

3. Experimental characterization and analysis

The WGMs within the functionalized microspheres were characterized using the experimental setup shown in Fig. 2(a). The output of a tunable laser diode (New Focus velocity 6300) was coupled into the microsphere using a $\sim 1 \mu\text{m}$ diameter fiber, which was fabricated using the flame heating method described in [17]. The wavelength of the tunable laser was controlled using the voltage signal produced by a function generator, where the 2 V (peak to peak) signal corresponded to a 0.16 nm tuning range. The photodetector converted the optical signals in the taper (after microsphere transmission) into electronic signals. The transmission spectra were then recorded by the oscilloscope. We used a fiber paddle to adjust the polarization state of the laser light in order to excite the WGMs with the highest Q factor. A representative example of WGM transmission spectrum is shown in Fig. 2(b), which includes a WGM with a Q factor of $\sim 1.5 \times 10^7$ obtained using a microsphere coated with a monolayer of PAH. From the measured transmission spectra, we can calculate WGM Q factors using [17]

$$Q = \frac{\lambda_R}{\Delta\lambda} \quad (1)$$

where λ_R and $\Delta\lambda$ are the central wavelength and the full width at half maximum of the measured transmission dips, respectively. For this paper, all Q factor measurements were carried out near 1550 nm and within a 0.16 nm scanning range. Furthermore, we always adjusted the polarization state of the input laser light to find the WGMs with the highest Q factors. If multiple WGMs were found within the 0.16 nm scanning range, we recorded the mode with the highest Q factor.

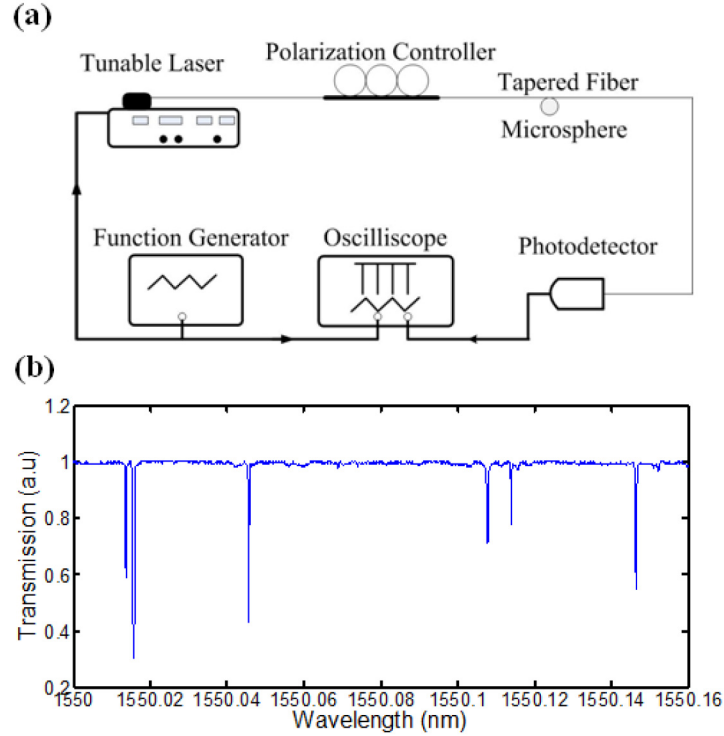


Fig. 2. (a) The experimental system for measuring the Q factors of functionalized silica microspheres. (b) Transmission spectrum of a silica microsphere coated with a monolayer of PAH.

3.1 Functional microspheres coated with ISAM films

The optical loss in a functional microsphere can come from several sources including optical absorption and Rayleigh scattering in silica, absorption in the ISAM film, scattering due to surface roughness, and taper-microsphere coupling [1,17]. Their contribution for cavity Q factors can be respectively represented by Q_{silica} , Q_{film} , Q_{ss} , and $Q_{coupling}$. Given the large microsphere sizes ($\sim 250 \mu\text{m}$), we can safely ignore the contribution due to radiation losses, which are exceedingly small when the ratio of microsphere diameter to resonator wavelength is greater than 15 [17]. We can then write the total cavity Q factor as

$$\frac{1}{Q} \approx \frac{1}{Q_{silica}} + \frac{1}{Q_{film}} + \frac{1}{Q_{ss}} + \frac{1}{Q_{coupling}} \quad (2)$$

Q_{silica} can reach 10^{11} when the resonance wavelength is around 1550 nm [17]. In contrast, as shown in Fig. 2(b), the experimentally measured Q factor of the functional microspheres can reach $\sim 1.5 \times 10^7$. Hence silica absorption should not be the main limiting factor. Another source for cavity loss is surface scattering of the ISAM film. According to [22], the Q factor due to surface scattering (Q_{ss}) can be estimated as:

$$Q_{ss} = \frac{3\varepsilon(\varepsilon + 2)^2 (\lambda_R)^{7/2} D^{1/2}}{4\pi^3 (\varepsilon - 1)^{5/2} \sigma^2 B^2} \quad (3)$$

where ε is material permittivity, D is the diameter of the microsphere, σ is the root-mean-square (rms) of the microsphere surface height variations and quantifies surface roughness, and B represents the correlation length of the random surface height variations.

In Fig. 3(a), we show the surface profile of a microsphere coated with 20 bilayers of PAH/PCBS obtained using an atomic force microscope (AFM). If we use $h(x, y)$ to denote surface height measured by AFM, we can define its correlation function as $R(u) = \iint h(x, y)h(x+u, y)dx dy$. The correlation length B can then be extracted by fitting the correlation function to $R(u) = R(0)\exp[-(u/B)^2]$ [23]. In Fig. 3(b), we show the experimentally obtained $R(u)$ as well as its fit to a gaussian form with $B = 11$ nm. Table 1 summarizes the data for different bilayer numbers of PAH/PCBS. The data include rms roughness, correlation length, and the corresponding estimate for Q_{ss} as given by Eq. (3). From the results in Table 1, Q_{ss} for microspheres coated with PAH/PCBS should be on order of 10^{10} to 10^{11} . This result suggest that for microspheres coated with PAH/PCBS, cavity loss is likely dominated by material absorption within the ISAM film and / or taper-microsphere coupling loss. Due to the difficulty of carrying out AFM measurements on a curved surface of mechanically fragile microspheres, we did not carry out similar studies using microspheres coated with PAH/PB. However, since deposition of PAH/PCBS and PAH/PB are carried out similarly and both ISAM films possess similarly smooth surface morphology on planar structures [24], the scattering losses for PAH/PB and PAH/PCBS microspheres are likely to be of the same order of magnitude.

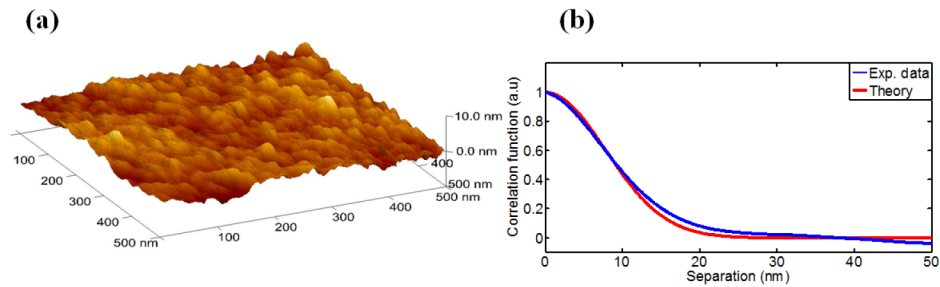


Fig. 3. (a) The surface profile of a functional microsphere coated with 20 bilayers of PAH/PCBS. The data was obtained using AFM. (b) The correlation of the surface profile of a microsphere coated with 5 bilayers of PAH/PCBS. Both experimental data (thin blue line) and theoretical fitting (thick red line) are shown.

Table 1. The rms surface roughness σ , correlation length B , and surface-scattering-induced Q factor (Q_{ss}) for three functional microspheres with different numbers of PAH/PCBS bilayer coatings.

Bilayer number	Surface roughness, σ (nm)	Correlation length, B (nm)	Q_{ss}
1	0.34	14	1.18×10^{11}
5	0.60	11	6.10×10^{10}
20	0.79	22	3.47×10^{10}

To further quantify the relationship between material absorption and cavity Q factors, we aim to minimize the impact of taper-microsphere coupling loss. To achieve this goal, all cavity Q factors were measured when the silica microspheres are in direct contact with the coupling taper. We first measured the Q factors of four different bare silica microspheres under this direct-contact scenario. The maximum cavity Q factors are respectively 1.73×10^7 , 1.88×10^7 , 1.95×10^7 , and 2.5×10^7 . The average Q factor is $\sim 2 \times 10^7$, with a standard deviation of 0.34×10^7 . All four bare silica microspheres possess similar diameters (~ 250 μm). For the

direct-contact cases, the cavity Q factors should be dominated by Q_{coupling} . Consequently, for functionalized microspheres with similar diameters, we can approximate their Q_{coupling} as $\sim 2 \times 10^7$.

The measured Q factors of microspheres coated with different numbers of PAH/PCBS and PAH/PB bilayers are shown in Fig. 4(a). We also fit the experimentally measured Q factor versus film thickness t using $1/Q = 1/Q_{\text{coupling}} + A \times t^\alpha$, where Q_{coupling} , A , and t are fitting parameters. Here we ignore cavity loss generated by silica absorption and surface scattering loss, as discussed earlier. In Fig. 4(b), we directly show Q_{film} (cavity Q factor due to film absorption) versus film thickness. The measured Q_{film} are obtained by subtracting the Q_{coupling} (determined by fitting in (a)) from the measured Q factor (Q_{coupling} is $\sim 1.96 \times 10^7$ for PAH/PB and is $\sim 1.93 \times 10^7$ for PAH/PCBS). We note that the fitted Q_{coupling} is very close to the Q_{coupling} of the bare microspheres given in the previous paragraph. The fitting curves are given by $1/Q_{\text{film}} = A \times t^\alpha$. For PAH/PB, the fitted α is +1.10 and for PAH/PCBS α is +1.14. A natural explanation for this result is that cavity loss of the functional microspheres is dominated by material absorption within the ISAM film. In this scenario, the cavity loss should increase linearly as a function of the total volume of the polymer coating. Since film thickness is approximately 1.3 nm per PAH/PB bilayer and 0.9 nm per PAH/PCBS bilayer, the rate of material absorption, which is represented by $1/Q_{\text{film}}$, should be proportional to the ISAM film thickness t , i.e., $1/Q_{\text{film}} \propto t$. This theoretical prediction is very close to our experimental results. The deviation from the theoretical fitting curve can be explained by several factors. First of all, the coupling between the fiber taper and the microsphere may not be identical for different microsphere samples. The geometrical dimensions of different microspheres may not be identical. The process of ISAM film deposition is not perfect clean, thus some dust particles may accumulate on the surface of the microsphere and cause the Q factor to drop in an uncontrollable fashion.

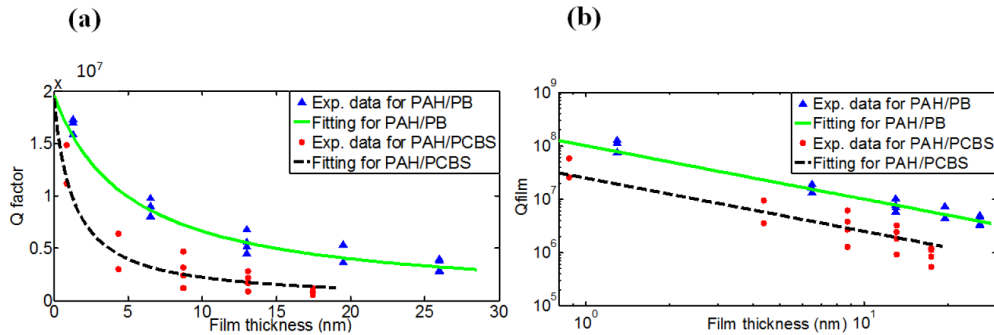


Fig. 4. (a) Total Q factors of the functional microsphere versus the self-assembled polymer layer thickness (t). The experimental data are shown as triangles (for PAH/PB) and dots (for PAH/PCBS). The theoretical fittings are performed using $1/Q = 1/Q_{\text{coupling}} + A \times t^\alpha$, where Q_{coupling} , A , and α are fitting constants. (b) The relationship between film thickness t and Q_{film} . The fitted values are given by $1/Q_{\text{film}} = A \times t^\alpha$. The experimental data are obtained using $1/Q_{\text{film}} = 1/Q - 1/Q_{\text{coupling}}$.

3.2 Functional microspheres coated with Au

To investigate the impact of Au NPs on WGM Q factors, we fabricated multiple microsphere samples covered with different amount of Au NPs. We can readily control the density of Au NPs by adjusting the duration of the self-assembly process, (i.e., deposition time). After sample fabrication, the Q factors of the microspheres covered with Au NPs were measured using the experimental system illustrated in Fig. 2(a). Subsequently, we took SEM images of the microsphere samples, and obtained NPs density from the SEM images. The measured microsphere Q factors were plotted as a function of NPs density, and shown in Fig. 5(b). As

expected, the cavity Q factors decrease as NP density increases. We can use the following theoretical model to describe the relationship between cavity Q factors and NPs density.

Let us first estimate the cavity Q factors associated with the self-assembled Au NPs (i.e., Q_{NP}). According to the definition of quality factors, we have:

$$Q_{NP} = \omega \frac{W}{P_{NPs}} \quad (4)$$

where ω is the angular frequency, P_{NPs} represents optical power loss induced by NPs scattering and absorption. W is the total energy stored within WGM, and can be written as [25]

$$W = \frac{1}{2} \iiint \epsilon_o \epsilon_r |\bar{E}_{WGM}(r, \theta, \phi)|^2 dV \quad (5)$$

where ϵ_o is the free space permittivity, ϵ_r is silica dielectric constant, and \bar{E}_{WGM} is the electric field of the WGM. To simplify theoretical analysis, we consider only TE modes, which leads to

$$W = \frac{1}{2k_o^2} \epsilon_o \epsilon_r \int [S(r)]^2 dr \iint |\bar{X}_{lm}(\theta, \phi)|^2 \sin \theta d\theta d\phi \quad (6)$$

where $\bar{X}_{lm}(\theta, \phi)$ is the angular vector function of WGM and its expression is explicitly given

in [26], and $S(r)$ represents radial dependence of the electric field. The integral $\int_0^R [S(r)]^2 dr$

can be approximated to $(R/2)(1 - \epsilon_o \epsilon_r^{-1})[S(R)]^2$ [25,27], where R is microsphere radius, and k_o is the free space wavenumber.

According to the definition of extinction cross-section, the power loss p_{NP} caused by a single Au NP on the silica microsphere surface can be estimated as

$$p_{NP} = \frac{|\bar{E}_{WGM}(R_i, \theta_i, \phi_i)|^2}{2\eta_o} \sigma_{ex} \quad (7)$$

where η_o is the free space impedance, $\bar{E}_{WGM}(R_i, \theta_i, \phi_i)$ is the electric field at the location of the i^{th} NP located on the surface, and σ_{ex} is the total extinction cross section area of the Au NP (includes both scattering and absorption). Assuming NPs are uniformly and randomly distributed over the microsphere surface, the total scattered and absorbed power from all particles on the surface, P_{NPs} can then be expressed by

$$P_{NPs} = \frac{N_p \sigma_{ex}}{2\eta_o} \iint |\bar{E}_{WGM}(R_i, \theta_i, \phi_i)|^2 dA \quad (8)$$

where N_p represents Au NP density. The integration is performed over the entire surface area A of the microsphere. For randomly distributed NPs, this equation can be simplified to

$$P_{NPs} = \frac{N_p \sigma_{ex}}{2\eta_o k_o^2} [S(R)]^2 \iint |\bar{X}_{lm}(\theta, \phi)|^2 \sin \theta d\theta d\phi \quad (9)$$

In the case of small Au NPs, the total (extinction) cross section can be written as [28]

$$\sigma_{ex.} = 4\pi a^2 x \operatorname{Im} \left\{ \frac{m^2 - 1}{m^2 + 2} \left[1 + \frac{x^2}{15} \left(\frac{m^2 - 1}{m^2 + 2} \right) \frac{m^4 + 27m^2 + 38}{2m^2 + 3} \right] \right\} + \frac{8}{3} x^4 \operatorname{Re} \left\{ \left(\frac{m^2 - 1}{m^2 + 2} \right)^2 \right\} \quad (10)$$

where m is the ratio of refractive index of the gold nanoparticles and air, and $x = 2\pi a / \lambda$. After combining Eqs. (4), (6), (9), and (10), we find Q_{NP} (generated by NP absorption and scattering) to be

$$Q_{NP} = \frac{\omega \epsilon_o \eta_o (\epsilon_r - 1) R}{2N_p \sigma_{ex.}} \quad (11)$$

In deriving Eq. (11), We have applied the procedures in [25,27,29]. Based on these results, the total Q factor of a silica microsphere covered with Au NPs can be estimated as

$$\frac{1}{Q} \approx \frac{1}{Q_{NP}} + \frac{1}{Q_{coupling}} \quad (12)$$

In deriving Eq. (12), we ignore cavity loss due to silica absorption, which is much smaller compared with losses due to Au NPs and taper-microsphere coupling. Furthermore, we note that according to Eq. (11), the NP-induced cavity loss is a simple function of microsphere radius, NP density, and NP extinction cross-section. Finally, we note that even though Eq. (11) is derived assuming TE modes, it should be able to provide a reasonable estimate for TM modes. This is because according to Eq. (9), the key factor that determines the NP-induced cavity loss is the electric field intensity at the microsphere surface, i.e., $[S(R)]$. Figure 5(a) show the radial dependence of two comparable TE and TM modes. As can be seen from the figure, the TE and TM modes have similar radial profiles. This implies that the NP-induced cavity loss should be of the same orders of magnitude for TE and TM modes.

Figure 5(b) shows the experimentally measured Q factors of NP-coated microspheres with different NP density. It also includes a theoretical estimate obtained using Eqs. (11) and (12). It should be mentioned that the theoretical predicted Q factors contain no fitting parameters. In particular, $Q_{coupling}$ is taken to be 2×10^7 , similar to that of bare microspheres. The radius of Au NPs is 15 nm. The refractive index of Au NPs at 1550 nm is $0.524 + i 10.72$, based on the data in [30]. Note that we don't take into account the enhanced absorption and scattering due to the plasmonic effects since the measurement is done at 1550 nm band, which is far from the plasmon resonance wavelength of Au [31]. Comparing theoretical predictions with experimental data, we note that the theoretically predicted Q factors can serve as a reasonable upper bound for the experimental results. Furthermore, we note that the theoretically predicted relationship between cavity Q factor and NP density is reasonably close to the experimental observed behavior. Such agreement is impressive, considering the fact that our theoretical predictions contain no free parameters. Finally, we note that the agreement between theory and experimental data is better for cases with low NP density. There are several possible explanations. For example, larger NP density corresponds to longer deposition time, which may potentially lead to more dust particles adsorbed onto the silica microsphere surface. Additionally, our model does not include the effect of particle aggregation on the surface. Particle aggregates scatter light much more efficiently than the individual particles do when separated, and this may also explain why the measured Q factors are lower than the predicted ones for higher surface particle densities.

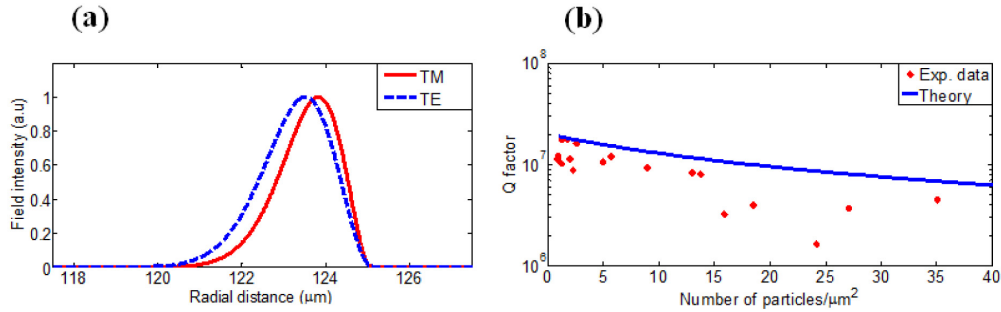


Fig. 5. (a) The radial dependence of a TE and a TM WGM. In our calculations, the radius of the microsphere is $125 \mu\text{m}$. The two angular modal numbers are $l = m = 715$ For the TM mode, and $l = m = 716$ For the TE mode. (b) The theoretically predicted and the experimentally measured cavity Q factors at different NP density levels. The theoretical results are calculated using Eqs. (11) and (12), and parameters given in the text.

4. Summary

In conclusion, we have investigated the Q factor of silica microsphere coated with thin film of nonlinear materials such as PB and PCBS as well as with sparsely adsorbed Au NPs. We find that scattering loss due to surface roughness is much smaller than the film absorption loss. In particular, the measured Q factors can be attributed two sources: one is taper-microsphere coupling; the other is optical absorption within the self-assembled polymers. Additionally, we demonstrate that it is possible to coat bare silica microspheres with 20 bilayers of PAH/PB or PAH/PCBS while maintaining cavity Q factor in the range of 10^6 . Finally, we analyze the reduction of cavity Q factor due to Au NPs adsorbed on the microsphere surface, and find reasonable agreement between theoretical estimates and experimental results.

Acknowledgments

We gratefully acknowledge support by the National Institute of Occupational Safety and Health (Grant No. 1U60OH009761-01) and the VT-MENA program and the U. S. Army Research Office under grant number W911NF-12-1-0026 for generous support.